November 2003 • NREL/CP-500-34297

Conference Paper

Wind Turbine Response to Analytic Inflow Vortex Parameters Variation

Preprint

M. M. Hand and M. C. Robinson
National Renewable Energy Laboratory

M. J. Balas
University of Colorado at Boulder

To be presented at the 23rd ASME Wind Energy Symposium
Reno, Nevada
January 5–8, 2004

National Renewable Energy Laboratory

1617 Cole Boulevard
Golden, Colorado 80401-3393

NREL is a U.S. Department of Energy Laboratory
Operated by Midwest Research Institute • Battelle • Bechtel

Contract No. DE-AC36-99-GO10337

WIND TURBINE RESPONSE TO ANALYTIC INFLOW VORTEX PARAMETER VARIATION

M. Maureen Hand
ASME Member
National Wind Technology Center
National Renewable Energy Laboratory
1617 Cole Blvd. MS 3811
Golden, Colorado 80401 USA
maureen_hand@nrel.gov

Michael C. Robinson
AIAA Member
National Wind Technology Center
National Renewable Energy Laboratory
1617 Cole Blvd. MS 3811
Golden, Colorado 80401 USA
michael_robinson@nrel.gov

Mark J. Balas
AIAA Fellow
Aerospace Sciences Center
University of Colorado
429 UCB
Boulder, Colorado 80309-0429 USA
mark.balas@colorado.edu

ABSTRACT*

As larger wind turbines are placed on taller towers, rotors frequently operate in atmospheric conditions that support organized, coherent turbulent structures. It is hypothesized that these structures have a detrimental impact on the blade fatigue life experienced by the wind turbine. These structures are extremely difficult to identify with sophisticated anemometry such as ultra-sonic anemometers. In order to ascertain the idealized worst-case scenario for vortical inflow structures impinging on a wind turbine rotor, we created a simple, analytic vortex model. The Rankine vortex model assumes the vortex core undergoes solid body rotation to avoid a singularity at the vortex center and is surrounded by a 2-dimensional potential flow field. Using the wind turbine as a sensor and the FAST wind turbine dynamics code with limited degrees of freedom, we determined the aerodynamic loads imparted to the wind turbine by the vortex structure. The size, strength, rotational direction, plane of rotation, and location of the vortex were varied over a wide range of operating parameters. We identified the vortex conformation with the most significant effect on blade root bending moment cycle amplitude. Vortices with radii on the scale of the rotor diameter or smaller caused blade root bending moment cyclic amplitudes that lead to reduced fatigue life. The rotational orientation, clockwise or counter-clockwise produces little difference in the bending moment response. Vortices in the XZ plane produce bending moment amplitudes significantly greater than vortices in the YZ plane. The response to vortices in the inflow is similar for both 2- and 3-blade turbines.

INTRODUCTION

The atmospheric boundary layer undergoes diurnal cycles that can support the generation and persistence of coherent, turbulent, vortex structures. It is hypothesized that these structures have a detrimental effect on the fatigue life of wind turbine structural components such as the blades [1-3]. We used experimental data obtained from the National Renewable Energy Laboratory's (NREL's) Long-Term Inflow and Structure Test (LIST) to establish a correlation between inflow parameters, such as Reynolds stresses, and wind turbine response, such as blade root flap bending moment. This correlation was not clearly identifiable with standard 10-minute record statistics [4]. Additional complicating variables included rotor teeter dynamics and blade pitch motion for power regulation. Although the unique inflow array, consisting of five sonic anemometers, provided more spatial resolution than that of previous experiments, the fidelity was insufficient to produce the detail necessary to establish this causal relationship. For these reasons, we explored this analytic approach of modeling vortical structures in wind turbine simulation codes.

Our study attempts to quantify the potential effect of vortex structures impinging upon a wind turbine. We developed a simple vortex model that convects at a specified mean wind speed. This analytic model was interfaced with the commonly used wind turbine aerodynamics model, Aerodyn [5]. The wind turbine structural dynamics code, FAST [6, 7], simulated the wind turbine response to the vortex. By restricting the degrees of freedom in the model to rotor rotation only,

* This work was performed at the National Renewable Energy Laboratory in support of the U.S. Department of Energy under Contract No. DE-AC36-99GO10337.

the turbine model isolated the aerodynamic load introduced by the vortex to the wind turbine blade. We used experimental data to establish an upper bound of circulation strength and vertical wind speed. We created response surfaces illustrating the blade root bending moment induced by vortices of varying radius, circulation, location with respect to the wind turbine hub, rotational direction, and plane of rotation. The similarity between aerodynamic response to a vortex from 2- and 3-blade turbines is demonstrated.

NOMENCLATURE

Δt	simulation time step, 0.004 s
B_o	constant for normalization of blade root bending moment, kNm
G or Γ	vortex circulation strength, m^2/s
G_o	constant for normalization of vortex circulation, m^2/s
ω	vorticity, s^{-1}
r	radial distance from vortex center to (x, y, z) position, m
CC	counter-clockwise rotation
CW	clockwise rotation
Q	dynamic pressure over rotor based on mean convection speed, Pa
ρ	air density, 1.00 kg/m^3 for sea level
R	radius of vortex, m
R_S	radius of circle formed by sonic anemometers, 21 m
R_T	radius of wind turbine, m
u,v,w	wind velocity components corresponding to x, y, z coordinates, respectively, m/s
V_∞	convection speed of vortex, m/s
x,y,z	blade element coordinates in aerodynamic code coordinate system, m
x_0, y_0, z_0	position of vortex center in aerodynamic code coordinate system, m

RANKINE VORTEX

The Rankine vortex is modeled as a potential vortex with a vortex core of variable radius undergoing solid body rotation to avoid a singularity at the vortex center. Parameters that are varied include the vortex radius, the circulation strength, the location of the vortex center with respect to the turbine hub, the orientation of the vortex flow, i.e. clockwise or counter-clockwise, and the plane in which the vortex rotates, i.e. XY, XZ, or YZ. Figure 1 is a diagram of the wind turbine coordinate system with a counter-clockwise rotating vortex in the XZ plane. Note that the origin is located at the intersection of the wind turbine tower centerline and the undeflected hub-height. If the vortex center is (x_0, y_0, z_0) in the aerodynamics code coordinate system, and the coordinates of the blade elements provided by the aerodynamics subroutine are (x, y, z), then the following equations describe velocity components at the (x, y, z) location that result from a vortex rotating clockwise in the XZ plane for r <= R:

$$u = -(z - z_0) + V_\infty \quad (1)$$

$$v = 0 \quad (2)$$

$$w = (x - x_0)\omega \quad (3)$$

The following equations describe the velocity components when r > R.

$$u = \frac{-\Gamma}{2\pi}\left(\frac{z - z_0}{(x - x_o)^2 + (z - z_0)^2}\right) + V_\infty \quad (4)$$

$$v = 0 \quad (5)$$

$$w = \frac{\Gamma}{2\pi}\left(\frac{x - x_o}{(x - x_0)^2 + (z - z_0)^2}\right) \quad (6)$$

The vortex convects at a specified mean wind speed from $-x$ to x by shifting x_0 by $V_\infty * \Delta t$ at every simulation time step. In the case of the vortex in the YZ plane, shown in Figure 2, the vortex convects laterally across the rotor from $-y$ to y by shifting y_0 by $V_\infty * \Delta t$ at every simulation time step. We selected 10 m/s for the convection speed for all simulations in this study. At this wind speed, the wind turbine operates below the rated wind speed where the aerodynamic performance is optimized.

To map the response of the wind turbine to vortices in the inflow, we varied the radius of the vortex and its circulation strength. The radius was varied from 1 m to 100 m to encompass a range that included scales of the turbine such as the blade chord (0.75 m) and the rotor radius (21.5 m). Using experimental data, we developed an upper bound for the circulation strength.

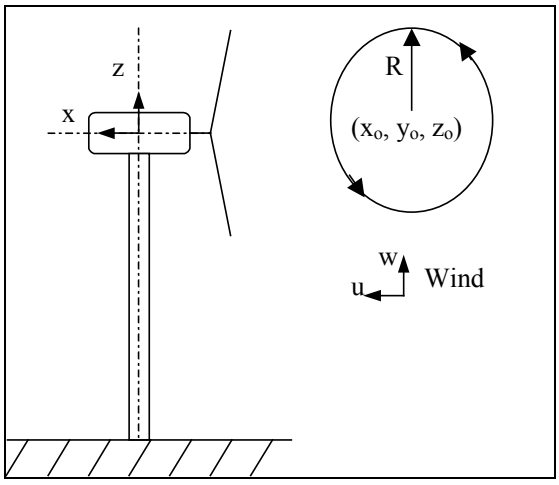

Figure 1: Wind turbine coordinate system with counter-clockwise rotating vortex of radius R in the XZ plane. The vortex convects to the left by adjusting x_o by $V_\infty * \Delta t$ at each simulation time step.

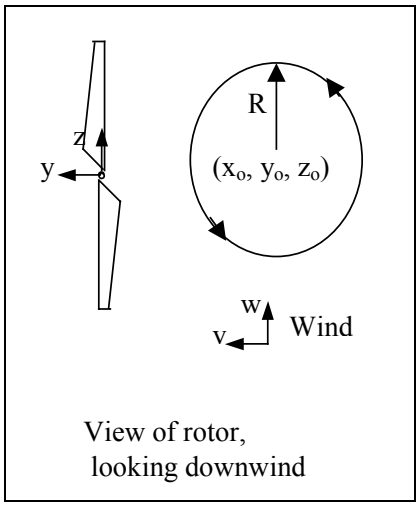

Figure 2. Wind turbine coordinate system with counter-clockwise rotating vortex of radius R in the YZ plane. The vortex convects to the left by adjusting y_o by V_∞ *Δt at each simulation time step.

EXPERIMENTAL DATA

We used data collected from the NREL's LIST to bound the simulated vortex circulation strength and vertical wind speed component. We conducted this field experiment at the National Wind Technology Center (NWTC) near Boulder, Colorado, from October of 2000 through May of 2001. A planar array consisting of five sonic anemometers located 1.5 diameter upwind of the Advanced Research Turbine (ART) collected 3-component wind velocities in 10-minute records at 40 Hz [8]. Figure 3 shows the inflow array. The ART is a 2-blade, upwind, 43-m diameter wind turbine with a teetered hub at 37 m [9, 10]. The blade root bending moments were measured with strain gages.

The spatial resolution of the four anemometers corresponding to the circumference of the rotor permit computation of the vorticity in the YZ plane according to the following equation:

$$\vec{\omega}_x = \left(\frac{\partial w}{\partial y} - \frac{\partial v}{\partial z} \right) \vec{i} \qquad (7)$$

The entire database of 10-minute records in which the turbine operated throughout the record, consisting of 1,941 records, was processed to obtain vorticity at each time step. The maximum and minimum values (positive suggests clockwise rotation, negative suggests counter-clockwise rotation from a reference point upwind of the turbine) were 0.38 s^{-1} and –0.43 s^{-1} respectively. These vorticity values correspond to circulation using the following relation where R_S represents the radius of the circle formed by the sonic anemometers, 21 m.

$$\Gamma = \int_A \vec{\omega}_x \cdot \vec{n} dA = \omega_x \pi R_S^{\,2} \qquad (8)$$

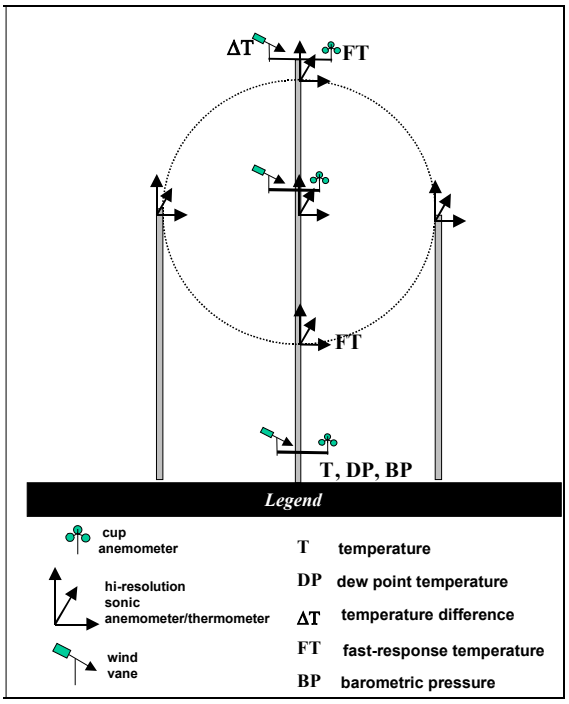

Figure 3. Inflow instrumentation array.

The highest circulation strength for a vortex in the YZ plane observed in the LIST experimental data was then 526 m^2/s or –582 m^2/s. Limiting this study to a maximum circulation of ± 1000 m^2/s provides a conservative overestimation of the circulation observed in the data. Because experimental data were not available to compute vorticity in other planes, we assumed that the circulation strength of vortex structures in the XY and XZ planes would not be substantially different from the circulation in the YZ plane.

Another restriction to the simulation parameters was based upon the vertical velocity component measured in the data. The maximum vertical velocity, *w* component, in the database of records where the turbine operated throughout each record was 12.2 m/s. By restricting the simulation to vortices where the vertical velocity component did not exceed 16 m/s, another conservative overestimation of observed flow parameters created a limit for simulation conditions. This limited the circulation for vortices of radius 1 m to 100 m^2/s, vortices of radius 3 m to 300 m^2/s, vortices of radius 5 m and 7 m to 500 m^2/s in addition to the restriction for all other radii introduced by the measured circulation strength, which was restricted to 1000 m^2/s.

Figure 4 graphically depicts the population of root flap bending moment range (difference between 10-minute record maximum and minimum) measurements for the entire database containing those records where the turbine operated throughout each record. The subset of those records corresponding to an average wind speed within the range 10 m/s ± 1 m/s is also included. The line in the center of the box represents the median value of the population. The box represents the lower and upper quartiles of the population. The whiskers extend to 150% of the inner quartile range. The outliers are represented by the '+' symbol. A similar graphical representation of the population of circulation strength maxima and the absolute value of the circulation strength minima are shown in Figure 5. Again, the entire database is contrasted with those records that fall within the 10 m/s mean wind speed bin for comparison.

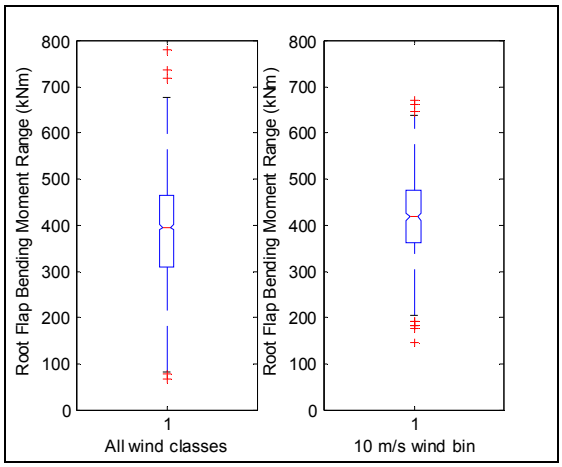

Figure 4. Root flap bending moment ranges from LIST experiment for all wind speed bins and for 10 m/s wind speed bin.

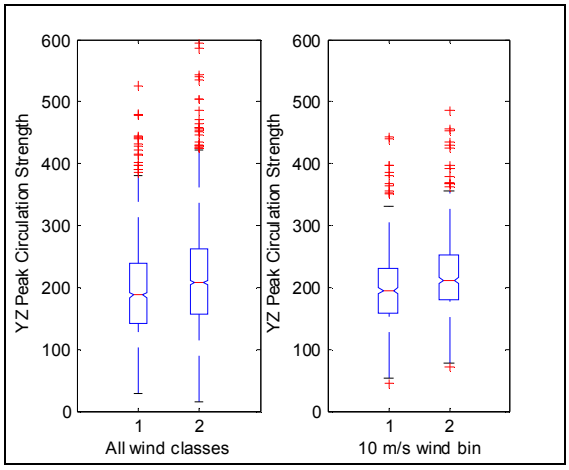

Figure 5. Circulation strength measured in YZ plane from LIST experiment for all wind speed bins and for 10 m/s wind speed bin. Maxima designated by 1; minima designated by 2.

WIND TURBINE SIMULATION

The wind turbine geometry simulated using the FAST code was that of the ART, a two-blade, teetered-hub, constant-speed wind turbine with blade pitch control to regulate power above rated wind speeds [9, 10]. This turbine has a rotor radius of 21.5 m and produces 600 kW at rated wind speeds. This simulation study restricted the modeled degrees of freedom to rotor rotation at a constant speed only. This limited degree-of-freedom turbine model allowed isolation of the aerodynamic forces imparted to the turbine by the vortex structure.

Because wind turbines are designed for optimal aerodynamic performance at rated wind speeds or lower, an operating point of 10 m/s was selected. The rated wind speed for the ART turbine is 12.9 m/s. If the ART operated at variable speed, the corresponding rotational speed at a wind speed of 10 m/s would be 37.1 RPM, and the corresponding pitch angle to achieve maximum power capture would be 1°. We specified the convection speed for the vortex to be 10 m/s for all simulations in this study to correspond to this turbine operating point. Under these conditions, the flow remains attached across the majority of the blade span except for the root section. Little lift is generated in this section due the relatively small chord length and generally cylindrical shape.

The aerodynamic loads were estimated using the AeroDyn subroutines incorporated in the FAST code. Dynamic stall was not simulated, and the equilibrium wake option was used. Minor modifications to the code permitted the inclusion of the vortex model in a fashion similar to the hub-height wind file option. In other words, the velocity components at each blade element were computed analytically at each time step using Eq. (1-6).

Simulations were run at the operating point mentioned above with several inflow vortex permutations. The vortex radius was varied from 1 m to 100 m. The circulation strength was varied from 10 m^2/s to 1000 m^2/s with additional restriction that resulted from the vertical velocity limitation for radii <= 7 m. The center of the vortex was varied from hub-height to the top of the rotor. We performed this series of 455 permutations using the models representing a vortex rotating in the YZ and the XZ plane for both clockwise and counter-clockwise orientation. We assumed that the XY vortex would be symmetric to the XZ vortex, and so it was excluded. The predicted blade root flap bending moment statistics, including mean, range (difference between maximum and minimum values), and standard deviation, were obtained for each simulation run.

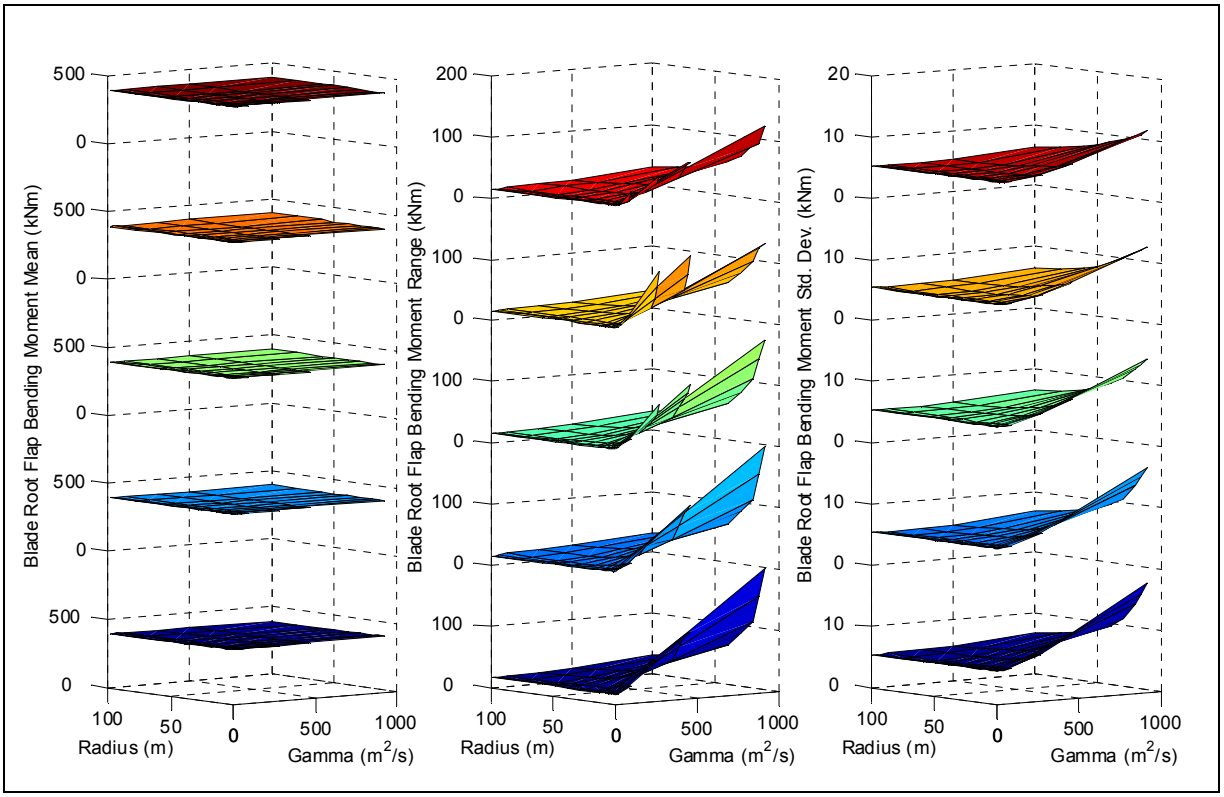

Figure 6: Clockwise rotating vortex in YZ plane with 10 m/s convection speed.

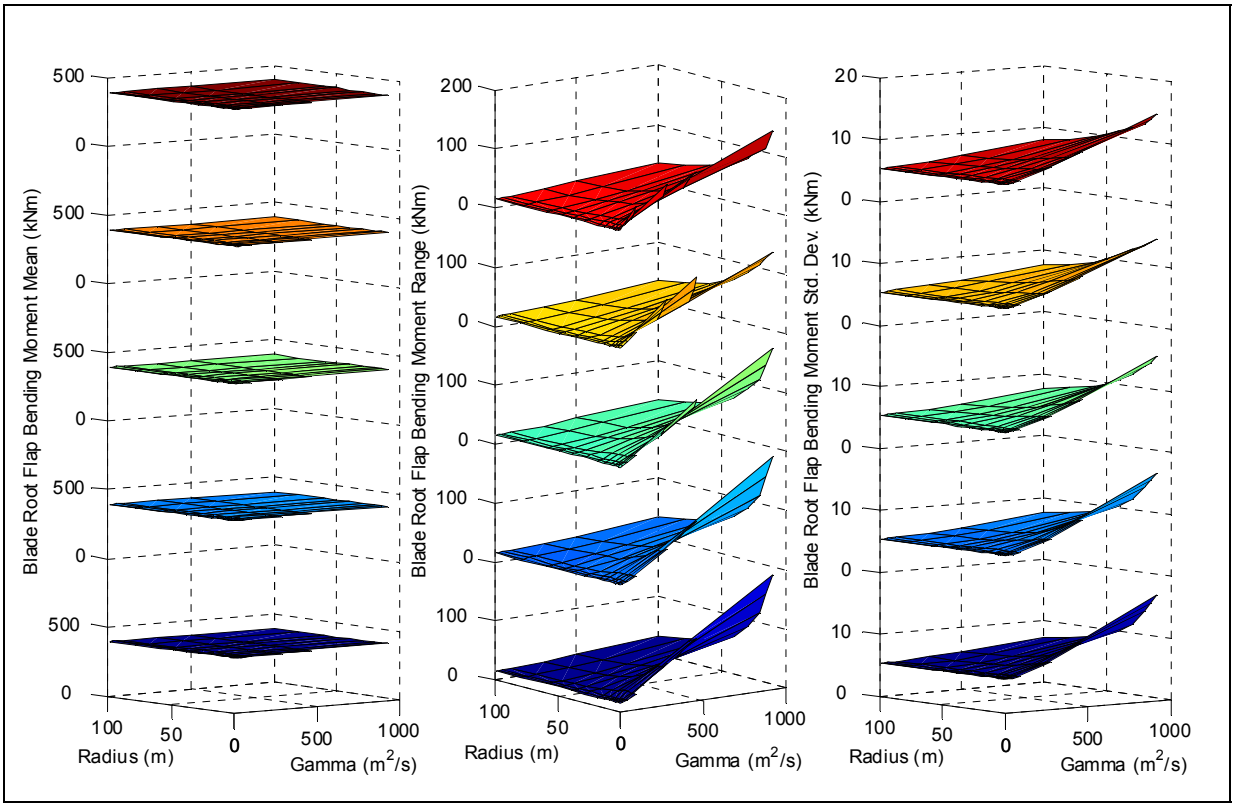

Figure 7: Counter-clockwise rotating vortex in YZ plane with 10 m/s convection speed.

WIND TURBINE RESPONSE TO VORTEX

To visualize the turbine response to relative vortex scale variations, we generated surfaces illustrating the blade root flap bending moment statistics. The mean, range, and standard deviation are shown in Figure 6 for the clockwise rotating vortex in the YZ plane. The vertical gradation of the surfaces represents the effect of shifting the vortex center with respect to the turbine hub height. The bottom surface represents a vortex centered at the hub (z_o=0 m); the upper surface represents a vortex centered at the top of the rotor plane (z_o=21.5 m); intermediate surfaces correspond to a vortex centered at equally spaced vertical positions along the blade between the hub and the tip. Similar surfaces representing a counter-clockwise rotating vortex in the YZ plane and a counter-clockwise rotating vortex in the XZ plane are shown in Figure 7 and Figure 8, respectively.

All surfaces show similarities in turbine response. The mean bending moment shows almost no variation with the scale and position of the vortex. The bending moment cyclic range and standard deviation, which contribute to fatigue damage, both increase as the radius of the vortex decreases and the circulation strength increases. Vortices with radii greater than 20-30 m appear to contribute very little to load variation. This suggests that vortices on the scale of the rotor (turbine radius = 21.5 m) or smaller produce the load variation that leads to fatigue damage.

The clockwise rotating vortex in the YZ plane has the same rotational orientation as the wind turbine, so the rotational velocity of the vortex adds to the rotational velocity of the wind turbine. Intuitively, one would expect higher loads when the velocities add as compared to the case where the velocities subtract, the counter-clockwise rotating vortex in the YZ plane. However, comparison of the bending moment range and standard deviation for both the clockwise and counter-clockwise rotating vortex in the YZ plane, Figure 6 and Figure 7, show similar magnitudes for the vortex centered at the hub. The counter-clockwise rotating vortex produces bending moment ranges exceeding those produced by the clockwise rotating vortex by approximately 20 kNm when the vortex is centered at the top of the rotor plane. In general, the loads produced when the vortex is centered at the hub are slightly higher than at any other location. Table 1 lists the magnitude of the bending moment ranges and standard deviations at the high magnitude edge for the surfaces that result from a vortex centered at the hub and a vortex centered at the top of the rotor. Figure 9 illustrates time series traces of the blade bending moment for the most extreme hub-height vortex in each rotation orientation. The center of the vortex passes through the wind turbine rotor at 120 s. The symmetric nature of the response explains the relatively small differences between the clockwise and counter-clockwise rotating vortices.

This symmetry also exists for vortices in the XZ plane, as illustrated in Figure 9. For this reason, surfaces representing only a clockwise rotating vortex in the XZ plane are presented in Figure 8. Table 1, however, lists the magnitudes for both orientations at the edge of the surface with the highest magnitude for comparison. For vortices centered at hub height, the counter-clockwise rotating vortex in the XZ plane has a steeper slope of blade bending moment range at the edge corresponding to small radius and high circulation strength. On average, both clockwise and counter-clockwise rotating vortices produce similar magnitude bending moment ranges for all vortex center locations. The vortex centered at the hub produces higher magnitude range loads than at any other vertical location. The bending moment range for a vortex centered at the top of the rotor plane produced about half the cyclic load as the vortex centered at the hub. However, the vortex centered at the top of the rotor could contribute to extreme peak loads. The vortex in the XZ plane produces cyclic range variations that exceed those produced by a vortex in the YZ plane by 2–10 times.

The highest magnitude bending moment range of 629 kNm that results from a vortex of 10 m radius and 1000 m^2/s circulation strength rotating counter-clockwise in the XZ plane compares favorably to the extreme range measured on the operating turbine in the 10 m/s wind speed bin shown in Figure 4. There are several complicating factors to this comparison. For example, the operating turbine has a teetered hub, and the measured blade bending moment could include the result of teeter stop impact. Also, the blade bending moment responds with higher cyclic fluctuation when the blade pitch is adjusted to regulate power production. Lastly, the mean wind speed over 10 minutes can fluctuate significantly, and the range statistic would not necessarily represent a single inflow event. The simulation does not include any pitch control or turbine dynamics in order to identify the aerodynamic load induced by a vortex in the inflow. Regardless, the relative magnitude of bending moment ranges produced by the simulated vortices compares favorably to those observed in the experimental data.

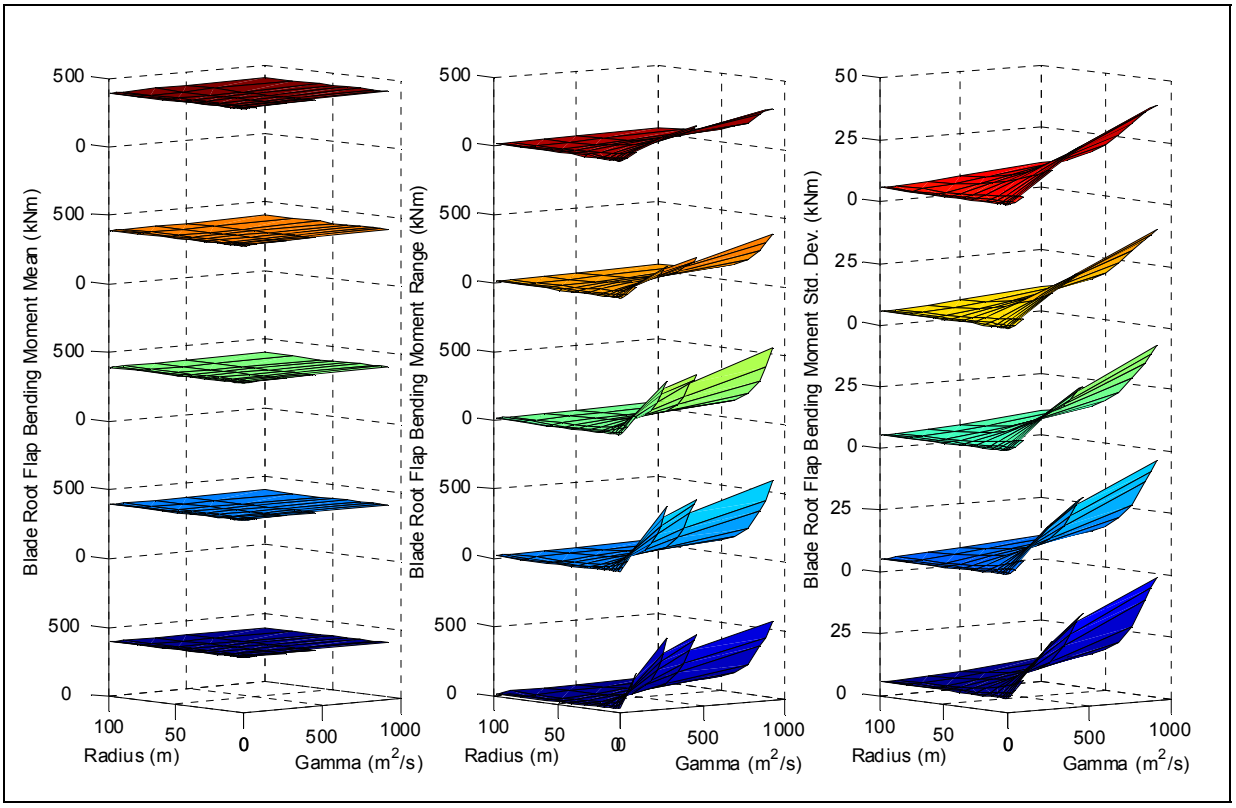

Figure 8: Clockwise rotating vortex in XZ plane with convection speed of 10 m/s.

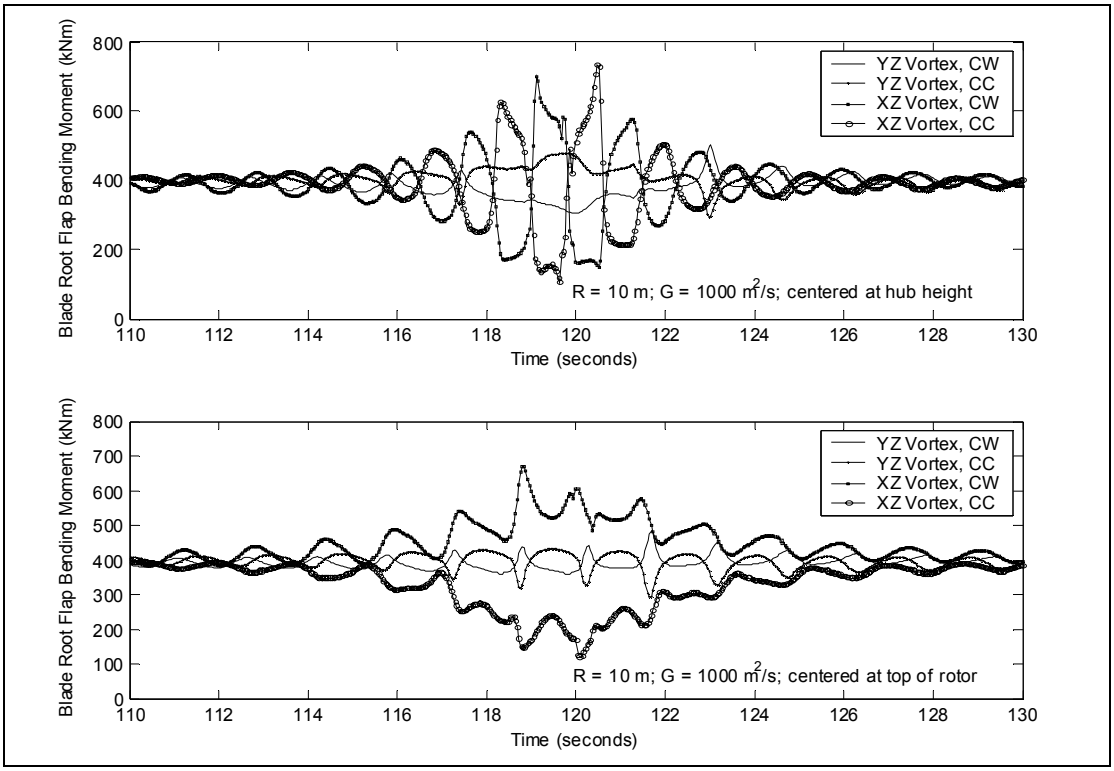

Figure 9. Time-series traces of simulated root flap bending moment that result from vortex passage.

We performed a preliminary investigation of approximating the vortex flow field by using the hub-height wind input file capability of the AeroDyn code. The horizontal, or *u*, velocity component produced by a 10 m radius, 500 m^2/s circulation vortex at the top and bottom of the rotor was used to compute a time varying, linear, vertical shear across the rotor. Similarly, we extracted the hub-height vertical, or *w*, velocity component from the vortex at each simulation time step. We used these values to create hub-height wind files that varied the vertical shear only, the vertical wind component only, and the combination of the two. Note that AeroDyn assumes specified vertical wind velocity components to be uniform across the entire rotor. Figure 10 illustrates the time-varying bending moment response to the vortex as well as these three approximations. The amplitude of the bending moment produced by the vortex exceeds all three approximations. The vertical shear alone most closely maintains the cyclic response and amplitude magnitude of the three approximations. However, the vortex model induces some cyclic bending moment variation at the peak amplitudes that is not captured by the approximations.

The aerodynamic response of a wind turbine to a vortex in the flow field should not be substantially different for 2- or 3-blade machines. This is demonstrated in Figure 11 where a dimensionless representation of the response surfaces for the bending moment coefficient range for the 2-blade turbine is compared to that of a 3-blade turbine where the vortex was centered both at the hub and at the top of the rotor. The 3-blade turbine model is a 46 m, 750 kW rotor based on an initial iteration from the WindPACT study [11]. It was modeled with only the rotor degree of freedom in the same manner as the 2-blade turbine model. The ratio of the vortex radius to the turbine radius is one parameter. The vortex circulation was normalized with the following parameter:

$$G_o = 2\pi R_T V_\infty \tag{9}$$

The blade root bending moment was normalized with the following parameter:

$$B_o = Q\pi R_T^{\,3} \tag{10}$$

where

$$Q = \frac{1}{2}\rho V_\infty^{\,2}. \tag{11}$$

The bending moment ranges for the 2- and 3-blade turbines are similar whether the vortex is centered at the hub or at the top of the rotor. The 3-blade turbine has a slightly steeper slope as the normalized radius is decreased and the normalized circulation is increased. However, the similarity in the aerodynamic response of the two turbines is confirmed.

CONCLUSIONS

This analytic study identifies the aerodynamic response of a wind turbine to analytic vortex structures in the inflow. The vortex variation included radius, circulation strength, location with respect to the hub height, orientation, and plane of rotation. We obtained blade response under each permutation through simulation using the FAST wind turbine dynamics code. The blade responses were presented in surface plots that illustrate the variations in blade load as a result of vortex passage through the rotor. Due to symmetry, the turbine response to clockwise and counter-clockwise rotating vortices was similar for vortices in the YZ and XZ planes. We assumed that this would also be true for vortices in the XY plane. A counter-clockwise rotating vortex in the XZ plane and aligned with the hub produced the greatest load variation. Decreased load variation was observed as the vortex was moved vertically to the top of the rotor plane, but these loads still exceeded those observed as a result of passage of a vortex in the YZ plane. It was assumed that vortices in the XY plane would be symmetric to those in the XZ plane. A vortex in the XZ plane is most representative of the type of vortical structure that could occur as a result of a Kelvin-Helmholtz instability in the atmospheric boundary layer in which the turbine operates. The mean bending moment is largely unaffected under any of these parameter variations. Vortices of radii less than 20–30 m, on the scale of the rotor or smaller, produce bending moment fluctuations that contribute to fatigue damage. Similar bending moment response is produced by a 3-blade turbine, as would be expected. Vertical shear across the rotor approximates the vortex induced bending moment cyclic variation more closely than the hub-height vertical wind component or a combination of vertical shear and vertical velocity. However, the amplitude of the vortex induced bending moment exceeds that of the vertical shear approximation.

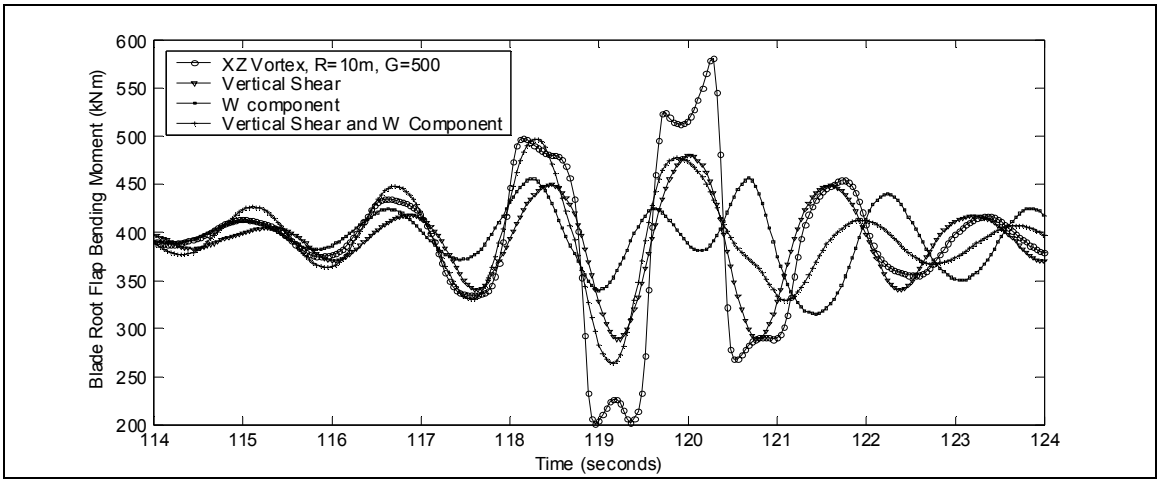

Figure 10. Comparison of wind field approximations of vortex with actual vortex induced bending moment.

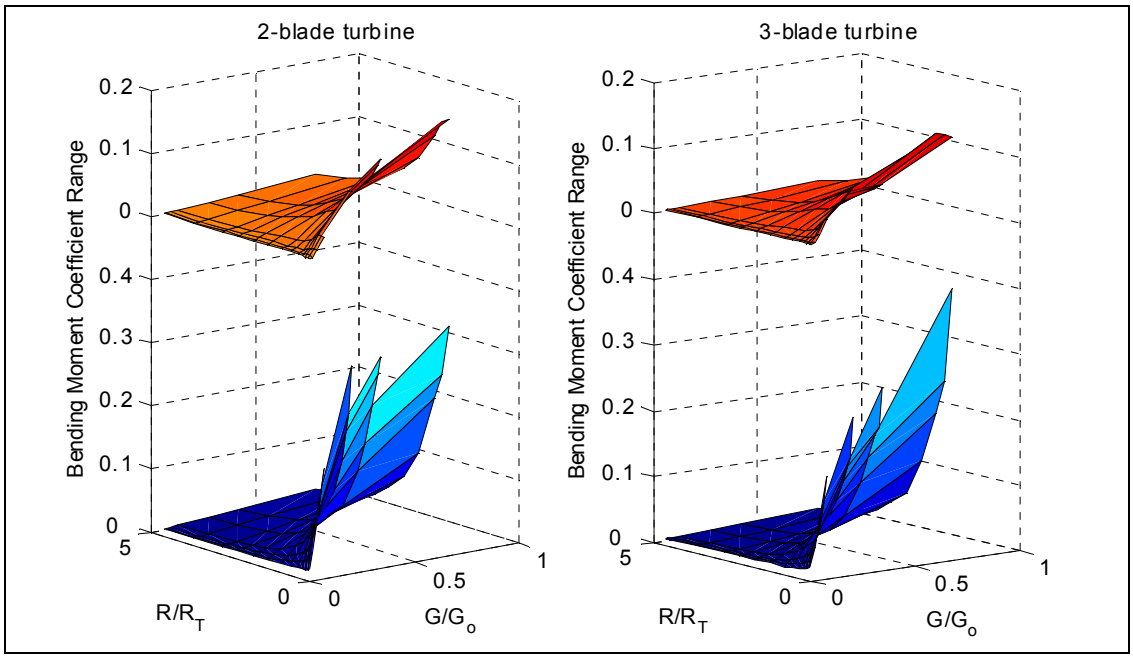

Figure 11. Comparison of dimensionless bending moment response to vortex passage from 2- and 3-blade wind turbine simulations.

FUTURE WORK

As degrees of freedom are added to the model, additional load fluctuation and associated vibration will be introduced. These additional degrees of freedom could enhance or damp the bending moment response due to vortex passage.

Using this insight into the characteristics of the most potentially damaging vortex scale, we will explore control algorithms to mitigate the response. Using the vortex model, we will develop a disturbance model for a Disturbance Accommodating Control (DAC) based controller.

REFERENCES

[1] Kelley, N.D., 1994, "The Identification of Inflow Fluid Dynamics Parameters that can be Used to Scale Fatigue Loading Spectra of Wind Turbine Structural Components," Proceedings, Wind Energy 1994, W. Musial et al., eds., American Society of Mechanical Engineers (ASME), New York, NY, SED-Vol. 15, pp. 181-196. NREL/TP-442-6008.

[2] Kelley, N.D., McKenna, H.E., 1996, "The Evaluation of a Turbulent Loads Characterization System," Energy Week Conference and Exhibition, 29 January-2 February, Houston, TX, ASME, New York, NY, Book VIII; pp. 69-77. NREL/TP-442-20164.

[3] Kelley, N.D., Bialasiewicz, J.T., Osgood, R.M., Jakubowski A., 2000, "Using Wavelet Analysis to Assess Turbulence/Rotor Interactions," *Wind Energy*, Vol. 3, pp.121-134.

[4] Hand, M.M, Robinson, M.C., Kelley, N.D., and Balas, M.J., 2003, "Identification of Wind Turbine Response to Turbulent Inflow Structures," Proceedings of the 4th ASME JSME Joint Fluids Engineering Conference, Renewable Energy Symposium, 6-10 July, Honolulu, Hawaii, ASME, New York, NY. NREL/CP-500-33465.

[5] Laino, D.J. and Hansen, A.C., 2002, "User's Guide to the Wind Turbine Aerodynamics Computer Software AeroDyn v.12.50", http://wind.nrel.gov/designcodes/aerodyn/aerodyn.pdf, last accessed September 24, 2003.

[6] Buhl, M.L., Jr, Jonkman, J.M., Wright, A.D., Wilson, R.E., Walker, S.N., Heh, P., 2003, *FAST User's Guide*, National Renewable Energy Laboratory, Golden, CO, NREL/EL-500-29798.

[7] Wilson, R. E.; Freeman, L. N.; Walker, S. N.; Harman, C. R., 1996, *Final Report for the FAST Advanced Dynamics Code: Two Bladed Teetered Hub Version 2.4 User's Manual Appendix for Three and Four Bladed Versions*, National Renewable Energy Laboratory, Golden, CO, NREL/SR-500-23563, 51 pp.

[8] Kelley, N., Hand, M., Larwood, S., McKenna, E., 2002, "The NREL Large-Scale Turbine Inflow and Response Experiment – Preliminary Results," Collection of the 2002 ASME Wind Energy Symposium Technical Papers Presented at the 40th AIAA Aerospace Sciences Meeting and Exhibit, 14-17 January, Reno, Nevada, ASME, New York, NY, pp. 412-426. NREL/CP-500-30917.

[9] Snow, A.L., Heberling, C.F., II, Van Bibber, L.E., 1989, *The Dynamic Response of a Westinghouse 600-kW Wind Turbine,* Solar Energy Research Institute, Golden, CO, SERI/STR-217-3405.

[10] Hock, S.M., Hausfeld, T.E., Thresher, R.W., 1987, *Preliminary Results from the Dynamic Response Testing of the Westinghouse 600-kW Wind Turbine*, Solar Energy Research Institute, Golden, CO, SERI/TP-217-3276.

[11] Malcolm, D. J.; Hansen, A. C., 2002, *WindPACT Turbine Rotor Design Study: June 2000--June 2002,* Work performed by GEC and Windward Engineering, National Renewable Energy Laboratory, Golden, CO, NREL/SR-500-32495, 82 pp.

Table 1: Simulated root flap bending moment values that result from vortex passage.

		Vortex in XZ plane, clockwise rotation		**Vortex in XZ plane, counter-clockwise rotation**		**Vortex in YZ plane, clockwise rotataion**		**Vortex in YZ plane, counter-clockwise rotation**	
		Range (kNm)	Std. Dev. (kNm)	Range (kNm)	Std. Dev. (kNm)	Range (kNm)	Std. Dev. (kNm)	Range (kNm)	Std. Dev. (kNm)
Z = hub height	R=1 m; G = 100 m^2/s	270	12.4	223	10.2	27	5.6	28	5.7
	R=3 m; G = 300 m^2/s	507	26.9	367	23.2	68	7.5	71	7.5
	R=5 m; G = 500 m^2/s	514	36.7	459	32.6	105	10.3	101	10.2
	R=10 m; G = 1000 m^2/s	551	48.3	629	47.4	199	17.4	185	16.8
Z = top of rotor plane	R=1 m; G = 100 m^2/s	64	8.2	84	8.5	38	5.2	53	5.9
	R=3 m; G = 300 m^2/s	164	17.8	194	20.1	57	5.9	81	7.6
	R=5 m; G = 500 m^2/s	226	26.0	226	29.6	76	7.3	93	9.6
	R=10 m; G = 1000 m^2/s	285	39.8	282	47.2	123	11.5	140	14.5

REPORT DOCUMENTATION PAGE

Form Approved
OMB NO. 0704-0188

1. AGENCY USE ONLY (Leave blank)	2. REPORT DATE	3. REPORT TYPE AND DATES COVERED
	November 2003	Conference Paper

4. TITLE AND SUBTITLE
Wind Turbine Response to Analytic Inflow Vortex Parameters Variation: Preprint

5. FUNDING NUMBERS
WER3.1940

6. AUTHOR(S)
M. M. Hand, M. C. Robinson, M. J. Balas

7. PERFORMING ORGANIZATION NAME(S) AND ADDRESS(ES)
National Renewable Energy Laboratory
1617 Cole Blvd.
Golden, CO 80401-3393

8. PERFORMING ORGANIZATION REPORT NUMBER
NREL/CP-500-34297

9. SPONSORING/MONITORING AGENCY NAME(S) AND ADDRESS(ES)

10. SPONSORING/MONITORING AGENCY REPORT NUMBER

11. SUPPLEMENTARY NOTES

12a. DISTRIBUTION/AVAILABILITY STATEMENT
National Technical Information Service
U.S. Department of Commerce
5285 Port Royal Road
Springfield, VA 22161

12b. DISTRIBUTION CODE

13. ABSTRACT *(Maximum 200 words)*
As larger wind turbines are placed on taller towers, rotors frequently operate in atmospheric conditions that support organized, coherent turbulent structures. It is hypothesized that these structures have a detrimental impact on the blade fatigue life experienced by the wind turbine. These structures are extremely difficult to identify with sophisticated anemometry such as ultra-sonic anemometers. In order to ascertain the idealized worst-case scenario for vortical inflow structures impinging on a wind turbine rotor, we created a simple, analytic vortex model. The Rankine vortex model assumes the vortex core undergoes solid body rotation to avoid a singularity at the vortex center and is surrounded by a 2-dimensional potential flow field. Using the wind turbine as a sensor and the FAST wind turbine dynamics code with limited degrees of freedom, we determined the aerodynamic loads imparted to the wind turbine by the vortex structure. The size, strength, rotational direction, plane of rotation, and location of the vortex were varied over a wide range of operating parameters. We identified the vortex conformation with the most significant effect on blade root bending moment cycle amplitude. Vortices with radii on the scale of the rotor diameter or smaller caused blade root bending moment cyclic amplitudes that lead to reduced fatigue life. The rotational orientation, clockwise or counter-clockwise produces little difference in the bending moment response. Vortices in the XZ plane produce bending moment amplitudes significantly greater than vortices in the YZ plane. The response to vortices in the inflow is similar for both 2- and 3-blade turbines.

14. SUBJECT TERMS
wind turbine; analytic vortex model; design codes; FAST; renewable energy

15. NUMBER OF PAGES

16. PRICE CODE

17. SECURITY CLASSIFICATION OF REPORT	18. SECURITY CLASSIFICATION OF THIS PAGE	19. SECURITY CLASSIFICATION OF ABSTRACT	20. LIMITATION OF ABSTRACT
Unclassified	Unclassified	Unclassified	UL